Unstable diffusion and chemical dissociation of a single sonoluminescing bubble

Joachim Holzfuss

Institut für Angewandte Physik, TU Darmstadt, Schloßgartenstrasse 7, 64289 Darmstadt, Germany
(Received 1 April 2004; published 9 February 2005)

In a certain parameter region, a single sonoluminescencing bubble is unstable against diffusion of gases and their chemical dissociation. Experiments show that a surface unstable bubble emits a microbubble and recoils. After this it exhibits specific dynamical features whereby the ambient radius changes in a nonmonotonic way. A numerical analysis identifies the phenomenon as the result of the interplay between spatial translations and induced variations of driving pressure on one side and the chemical composition of gases in the bubble on the other side. The results confirm that dynamical chemical dissociation phenomena as well as acoustic properties play an important role in the understanding of single-bubble sonoluminescence.

Single-bubble sonoluminescence (SBSL) is the phenomenon of a single bubble in water driven in an ultrasound field emitting light flashes upon a violent collapse [1,2]. One of the astonishing facts is that the pulsations and light emissions can be made very stable and last for hours. This stability is astonishing since it has been known for a long time that during bubble oscillations diffusion of gases from the surrounding fluid through the bubble wall is present. Because the pressure in the bubble oscillates by more than ten orders of magnitude the partial pressure of gases in the bubble should also be changing. Early theoretical papers [3] realized that in the SBSL parameter space a bubble should be constantly growing due to rectified diffusion since the high pressures occur during only a very short time interval of the whole oscillation period. Experiments showed that an air bubble is stable if the gas concentration in the liquid is 1% of the value set in the experiment [4]. In [5] it was proposed that due to the high temperatures at bubble collapse chemical dissociation of noninert gases gives rise to the formation of highly soluble species that immediately dissolve in the surrounding water leaving only argon (1% of air) in the bubble. Further experiments [6] underlined the finding that mostly argon is present. Parameter regions are identified where a bubble is stable against diffusion and dissociation. In these experiments the gas concentration in the liquid and driving sound pressure are fixed and it is seen that the bubble chooses an adequate ambient radius that can be measured. Stability curves are drawn in the parameter space representing a stable oscillating bubble.

In the upper driving pressure range at higher dissolved gas concentrations the bubble is no longer stable [1,7]. The ambient radius of the fast oscillating bubble is growing due to diffusion on a slow time scale until the bubble breaks up by microbubble splitoff. Normally a bubble with small ambient radius survives, which then increases until the whole process repeats. The breakup is explained by the fact that an argon bubble reaches a parametric instability threshold where surface waves are amplified leading to a sudden removal of bubble volume. A close inspection of the time evolution near this instability, however, shows that the process is more involved (Fig. 1). The relative collapse time, the time difference between collapse and a constant phase of the driving, is calculated from shock wave recordings [8]. It is a measure for the ambient bubble radius. Figure 1 shows the slow increase in relative collapse time followed by bubble splitoff. Immediately after the breakup a fast increase of the collapse time followed by a rapid decrease is seen, after which it increases again monotonically.

This peak during diffusionally unstable SBSL is shown to be the result of a combined instability effect. A sonoluminescing bubble consisting solely of argon loses some of its volume at microbubble splitoff thereby undergoing a sudden spatial dislocation (recoil). Translating back to the antinode of the sound pressure field it is moving through a complex phase space during which the chemical composition of its gas contents changes drastically. This effect demonstrates a dynamical variant of the argon hypothesis [5]. For a further explanation we have to look more closely at bubbles during bubble splitoff. Figure 2 shows a series of images of a big bubble emitting a small bubble near the lower SBSL threshold. The small bubble is leaving the split-off site at a decreasing speed and dissolves. The bigger part of the bubble experiences a recoil and subsequent return, denoted by some authors as "dancing." Figure 3 shows a double-exposed image of two shock waves emitted during bubble collapse, one before and one after the microbubble splitoff at the upper SBSL threshold. The centers of the circular structures are shifted with respect to each other due to a recoil or spatial translation. The radii of the shock waves differ. A larger radius means a larger time between shedding of the shock at collapse and the following phase locked illumination flash. Smaller bubbles have an earlier collapse and are thus identified by a larger shock wave radius. From the position of the centers of the two shock waves of Fig. 3 a lower bound of the translational velocity during splitoff of 0.5 m s⁻¹ can be calculated [8]; the change of shock wave radius resulting in a change of collapse time of 1 μs shows the volume loss.

A numerical analysis of the dynamics of a diffusionally unstable SBSL bubble uses a model consisting of equations for radial motion of the bubble wall, gas diffusion through the bubble wall, chemical dissociation of noninert gases, and translational movement of the bubble in a sound pressure gradient. The Gilmore model [9] describing the radial motion of a bubble in a compressible liquid is integrated numerically:
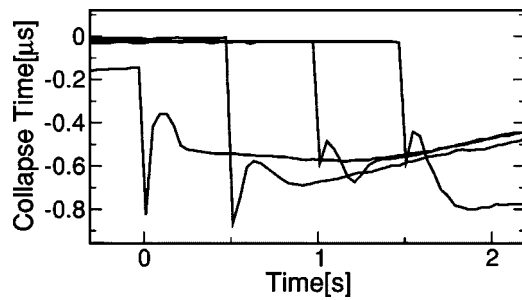
FIG. 1. Relative collapse time during bubble splitoff of diffusionally unstable sonoluminescing bubble (experiment). Successive split-off curves have been collected; their time scale has been shifted for superposition. The collapse times are shown relative to the largest one, which is set to 0.

$$\left(1 - \frac{\dot{R}}{C}\right)R\ddot{R} + \frac{3}{2}\left(1 - \frac{\dot{R}}{3C}\right)\dot{R}^2 = \left(1 + \frac{\dot{R}}{C}\right)H + \left(1 - \frac{\dot{R}}{C}\right)\frac{R}{C}\frac{dH}{dt},$$

(1)

$$H = \int_{p_\infty}^{p(R,\dot{R})} \rho^{-1} dp, \quad \frac{p+B}{p_0+B} = \left\{\frac{\rho}{\rho_0}\right\}^n,$$

(2)

$$C = c|_{r=R} = \left.\sqrt{\frac{dp}{d\rho}}\right|_{r=R} = c_0\left(\frac{p(R,\dot{R})+B}{p_0+B}\right)^{(n-1)/2n},$$

$$p(R,\dot{R}) = p_g(R) - \frac{2\sigma}{R} - \frac{4\eta}{R}\dot{R},$$

$$p_g(R) = \left(p_0 + \frac{2\sigma}{R_0}\right)\left(\frac{R_0^3 - b^3}{R^3 - b^3}\right)^\gamma.$$

(3)

R is the bubble radius, and C, ρ, and $p(R,\dot{R})$ are the speed of sound in the liquid, its density, and the pressure at the bubble wall, respectively. p_g is the pressure in the bubble. H is the enthalpy difference of the liquid at pressure p_∞ and $p(R,\dot{R})$ at the bubble wall. p_∞ is the pressure at infinity taken as $p_\infty = p_0 + p_A\cos(2\pi ft)$, $p_0 = 1$ atm. The driving frequency f is 23.5 kHz, and the driving amplitude is set by a standing wave $p_A = p_{A_0}\cos(kz)$, z pointing against the direction of the gravity vector. The special choice of the wave vector $k = 2\pi/2\lambda$, where λ is the wavelength in water, reflects the experimentally observed mode [8,10,11]. Parameters were set to $c_0 = 1483$ m s^{-1}, $\sigma = 0.0725$ N m^{-1}, $\eta = 0.001$ N s m^{-2}. b is the van der Waals hard-core radius and γ a polytropic exponent. Its value is set between 1 (isothermal) and the adiabatic exponent of the gas $(f+2)/f$ being the respective degrees of freedom) according to the instantaneous Péclet number [5,12] Pe$= R_0^2|\dot{R}(t)|/R(t)\kappa$, κ being the thermal diffusivity of the gas, reflecting thermal conduction at the involved time scales. To avoid a change to isothermal behavior at the bubble wall turning point during maximum compres-
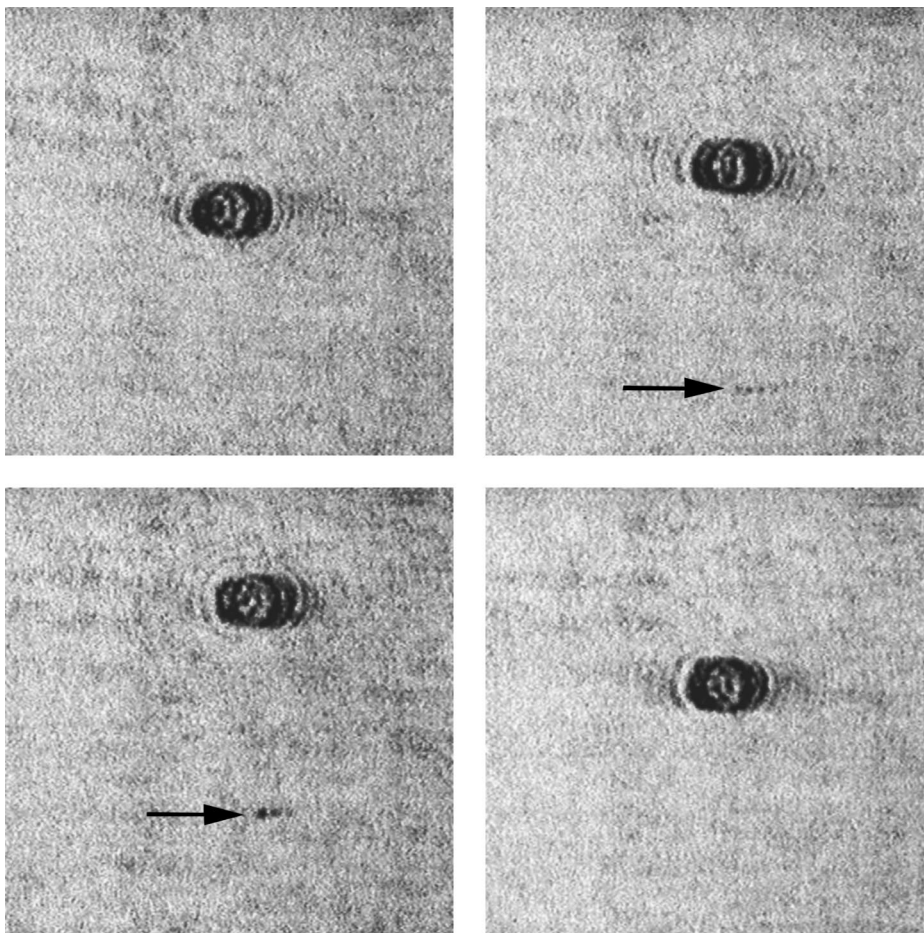
FIG. 2. Series of images of a bubble emitting a small bubble. Image side length is 0.512 mm; interframe time is 40 ms.
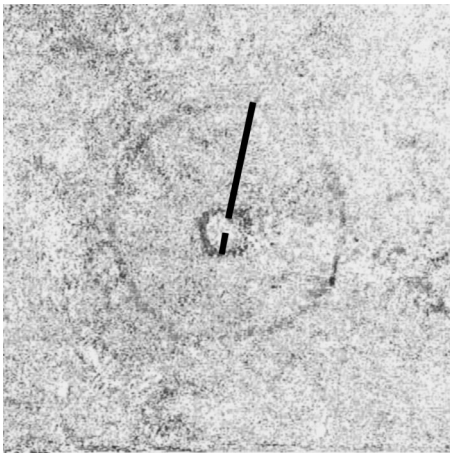
FIG. 3. Double-exposure image of shock waves shed during bubble collapse before and after bubble splitoff. The lines are radii. Image side length is 3.916 mm; upper bound of the time between exposures is 0.255 ms.

sion, Pe and γ(Pe) are kept constant at their respective values during positive bubble wall accelerations. b and γ are updated during calculations to reflect the actual gas content. The Tait equation is taken as the equation of state for water using $n=7.025$, $B=3046$ bar [8] as parameters. The number of moles of the different species in the bubble n_i is changed by diffusion of air dissolved in the water. The solution of the diffusion equation is

$$\dot{n}_i^{diff} = 4\pi R^2 \frac{1}{M_i} D_i \frac{\partial C_i(r)}{\partial r}\bigg|_{r=R}. \qquad (4)$$

M_i, D_i, and C_i are the individual molar masses, diffusion constants, and concentration fields, $i=N_2$, O_2, Ar. The concentration of species at the bubble wall is assumed to connect to the partial pressures p_i inside according to Henry's law: $C_i|_{r=R}=C_i^0 p_i(R)/p_0$. Because of the slow diffusional timescale the adiabatic approximation [13] can be employed and the change per period T is

$$\frac{\Delta n_i^{diff}}{T} = \frac{4\pi D_i C_0^i R_{max}}{M_i p_0} = \left(p_i^\infty - \left\langle \frac{n_i}{n_0} p_g(R) \right\rangle_4\right), \qquad (5)$$

where n_0 is the sum of moles of all molecules in the bubble and $\langle f(t)\rangle_i = \int_0^T f(t) R^i(t)dt / \int_0^T R^i(t)dt$ are weighted time averages. Chemical dissociation occurs for noninert gases [5,14–16] and reaction products are immediately diffused into the liquid. The dissociation per period is calculated as a second-order reaction by a modified Arrhenius law:

$$\frac{\Delta n_i^{diss}}{T} = -n_i \left\langle \frac{n_0}{\frac{4}{3}\pi R^3} w A_i \left(\frac{T_B}{T_0}\right)^{\beta_i} e^{-E_A^i/(R_{gas}T_B)} \right\rangle_0. \qquad (6)$$

A_i and β_i are Arrhenius constants [17] and E_A^i activation energies. $R_{gas}=8.3143$ J mol^{-1} K^{-1} is the gas constant, and $T_B=T_0[(R_0^3-b^3)/(R(t)^3-b^3)]^{\gamma-1}$ the bubble temperature, $i=N_2,O_2$. $w=(1-x)e^{-x/(1-x)}$, $x=\lambda R^3/b^3$, limits the dissociation rate to reflect an excluded volume [16]. $\lambda \in [0,1]$ is introduced to gradually control this high-pressure limit. A value of $\lambda=0.85$ is taken, as justified by the results.

Evaporation and condensation of water molecules at the bubble wall [14,15] is included in the model, as experimental results [18] stress the importance of a decrease of the polytropic exponent at bubble collapse. A simple Hertz-Knudsen model for the change of moles of water vapor is

$$\dot{n}_{H_2O} = \dot{n}_{H_2O}^{evap} - \dot{n}_{H_2O}^{cond} = \frac{4\pi R^2 \alpha}{M_{H_2O}} \frac{\bar{c}(T_s)}{4} [\rho_{g,H_2O}^{sat} - \rho_{g,H_2O}(R)], \qquad (7)$$

where $\alpha=0.4$ is the evaporation coefficient [19], $\bar{c}(T_s)=\sqrt{8R_{gas}T_s/(\pi M_{H_2O})}$ is the average velocity of molecules, ρ_{g,H_2O} is the density of water vapor in the bubble, and $\rho_{g,H_2O}^{sat}=0.0173$ kg m^{-3} is the saturated vapor density. The bubble surface temperature is $T_s=T_0$.

To model bubble translations (Figs. 2 and 3) an equation for the radius and time-dependent buoyancy and Bjerknes force, change of effective bubble mass in the liquid, and drag force is added:

$$m_{eff}\dot{v} = F_{bouyancy} + F_{dmdt} + F_{Bjerknes} + F_{drag},$$

$$\left(\frac{\rho_l}{2} + \rho_g(t)\right)V(t)\dot{v}(t) = 9.81[\rho_l - \rho_g(t)]V(t)$$
$$-2\pi R(t)^2\rho_l\dot{R}(t)v(t) - V(t)\nabla p(z,t)$$
$$-\frac{3}{8}\rho_l V(t)c_D(t)v(t)|v(t)|. \qquad (8)$$

The velocity of the bubble in the liquid is $v(t)$, $V(t)$ is the bubble volume, $\rho_l=\rho_0$ the liquid density, and ρ_g the respective gas density of the bubble. The drag coefficient $c_D=24/\text{Re}$ for small Re results in the Stokes drag; Re $=2Rv(t)\rho_l/\eta$ is the Reynolds number for the bubble translation. For larger Re a slightly modified expression [20] $c_D=27/\text{Re}^{0.78}$ is used. To accomplish continuity of the drag force, the expressions are switched at the crossing point (Re≈ 0.585). As the largest translations occur at higher Reynolds numbers, the addition of a Bassett type history force can be neglected [21]. A varying hydrostatic pressure by vertical translations is added to p_∞ as $p_h=9.81\rho_l(z_h-z)$, $z_h=0$.

The numerical simulation starts after bubble splitoff at the upper threshold for SBSL, as a small remaining argon bubble has been shifted by recoil and is translating back into the pressure antinode (Figs. 4 and 5): In the beginning the sound pressure is low and the bubble temperature is small such that N_2 and O_2 molecules diffusing into the bubble are not dissociated. As a consequence the bubble volume (ambient radius) increases (Fig. 5). On its way to the center, driving pressure and temperature increase and dissociation sets in (Fig. 4). The ambient bubble radius is decreasing as the reaction products are diffusing into the liquid. Only the inert argon remains, while the ambient bubble radius is still growing due to diffusion. When the upper SBSL threshold for parametric instability [22] is reached (Fig. 5), the process can repeat. Figure 5 shows bubble paths for different start sizes and recoil distances. Larger recoil distances display a larger
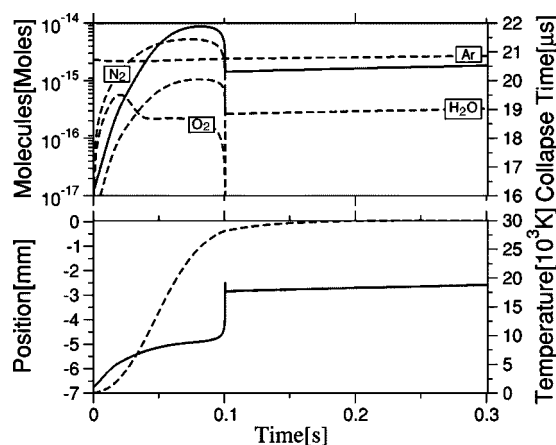
FIG. 4. Numerical calculation of bubble properties after splitoff with a recoil jump of -7 mm: a small remaining (2 μm) Ar bubble is attracted by the antinode ($P_A = 1.28$ bar). Upper graph: Collapse time (straight line) and chemical composition of bubble (dashed lines). Lower graph; position (dashed) and temperature in the bubble (straight). All data are taken at minimum radius.

FIG. 5. Phase space spanned by driving pressure and bubble ambient radius (taken at the negative sloped zero crossing of the driving), stability lines, and paths of some bubbles after splitoff. The upper shaded area covers the parametric instability region of a vapor-filled argon bubble; above the lower shaded area is the region for diffusive growth calculated for an air-vapor bubble (40% ambient concentration). The dashed **C**-shaped line encloses the region of diffusive growth of an argon-vapor bubble (0.4% ambient Ar concentration). Bubble paths for recoils of -5, 5, and -6 mm (dotted, bottom to top), and -7 mm (same data as in Fig. 4) are shown.

variation in equilibrium size and collapse time. While the calculated time scales of the width of the peak agree with the experiment, the dissociation dominated side is less steep in the experiment (Fig. 1) than in the simulation (Fig. 4). This suggests that a substantial amount of reaction products with small diffusion constants is produced. The dissociation rates have to be limited at the very high pressures involved around the peak (from 0.3 to 138 kbar dropping to 90 kbar at splitoff), else the peak duration is an order of magnitude too small. The λ factor in the dissociation limiting function has to be smaller than 1, else the high pressures inhibit dissociation of air in this model. Bubbles with an upward pointing recoil display higher temperatures and shorter peaks at the decreased hydrostatic pressure. The results show that diffusion together with chemical kinetics and translatory dynamics as a dynamical application of the dissociation theory [5] explain the details of a diffusionally unstable SBSL bubble.

The results suggest that spectra of the light emission of diffusionally unstable sonoluminescing bubbles change during the cycle from a line dominated spectrum to bremsstrahlung. It is supposed that this also holds true for the spectra difference of stable SBSL argon bubbles and multibubble sonoluminescence. Small bubbles approaching pressure antinodes along streamers grow by diffusion of air and stay too cold to dissociate much of their contents before they get surface unstable, split, and recycle.

[1] D. F. Gaitan, L. A. Crum, C. C. Church, and R. A. Roy, J. Acoust. Soc. Am. **91**, 3166 (1992).

[2] B. P. Barber and S. J. Putterman, Nature (London) **352**, 318 (1991); B. P. Barber, R. A. Hiller, R. Löfstedt, S. J. Putterman, and K. R. Weninger, Phys. Rep. **281**, 65 (1997).

[3] R. Löfstedt, K. Weninger, S. Putterman, and B. P. Barber, Phys. Rev. E **51**, 4400 (1995),

[4] R. G. Holt and D. F. Gaitan, Phys. Rev. Lett. **77**, 3791 (1996).

[5] D. Lohse, M. P. Brenner, T. F. Dupont, S. Hilgenfeldt, and B. Johnston, Phys. Rev. Lett. **78**, 1359 (1997); D. Lohse and S. Hilgenfeldt, J. Chem. Phys. **107**, 6986 (1997).

[6] B. P. Barber, K. Weninger, R. Löfstedt, and S. Putterman, Phys. Rev. Lett. **74**, 5276 (1995); J. A. Ketterling and R. E. Apfel, *ibid.* **81**, 4991 (1998); T. J. Matula and L. A. Crum, *ibid.* **80**, 865 (1998); S. J. Putterman and K. R. Weninger, Annu. Rev. Fluid Mech. **32**, 445 (2000); Y. T. Didenko and K.

S. Suslick, Nature (London) **418** 394 (2002).

[7] S. Hilgenfeldt and D. Lohse, Phys. Fluids **8**, 2808 (1996).

[8] J. Holzfuss, M. Rüggeberg, and A. Billo, Phys. Rev. Lett. **81**, 5434 (1998).

[9] F. R. Gilmore, California Institute of Technology Report No. 26-4, 1952 (unpublished).

[10] M. Rüggeberg, *Stoßwellenemission und die Akustische Umgebung einer Sonolumineszierenden Blase* (Shaker, Aachen, 2000).

[11] J. Holzfuss, M. Rüggeberg, and R. Mettin, Phys. Rev. Lett. **81**, 1961 (1998); J. Holzfuss, M. Rüggeberg, and R. G. Holt, Phys. Rev. E **66**, 046630 (2002); J. Holzfuss and M. Rüggeberg, *ibid.* **69**, 056304 (2004).

[12] A. Prosperetti, J. Acoust. Soc. Am. **61**, 17 (1977).

[13] M. M. Fyrillas and A. J. Szeri, J. Fluid Mech. **277**, 381 (1994).

[14] B. D. Storey and A. J. Szeri, Proc. R. Soc. London, Ser. A **456**,

1685 (2000); Phys. Rev. Lett. **88**, 074301 (2002).

[15] K. Yasui, J. Phys. Soc. Jpn. **66**, 2911 (1997); V. Kamath, A. Prosperetti, and F. N. Egolfopoulos, J. Acoust. Soc. Am. **94**, 248 (1993); M. P. Brenner, S. Hilgenfeldt, and D. Lohse, Rev. Mod. Phys. **74**, 425 (2002).

[16] R. Toegel and D. Lohse, J. Chem. Phys. **118**, 1863 (2003).

[17] $\left[A_i \ (\mathrm{m^3 \ mol^{-1} \ s^{-1}}), \beta_i, E_A^i/R_{gas} \ (\mathrm{K})\right]$ for N_2 $(5.55 \times 10^{13},$ 2.5, 113 000); O_2 $(5.3716 \times 10^9,$ 1.0, 59 400), from NIST kinetics database, http://kinetics.nist.gov

[18] G. E. Vazquez and S. J. Putterman, Phys. Rev. Lett. **85**, 3037 (2000); R. Toegel, B. Gompf, R. Pecha, and D. Lohse, *ibid.*

85, 3165 (2000).

[19] I. W. Eames, N. J. Marr, and H. Sabir, Int. J. Heat Mass Transfer **12**, 2963 (1997),

[20] L. A. Crum, J. Acoust. Soc. Am. **57**, 1363 (1975).

[21] J. Magnaudet and D. Legendre, Phys. Fluids **10**, 550 (1998); A. J. Reddy and A. J. Szeri, J. Acoust. Soc. Am. **112**, 1346 (2002); T. J. Matula, *ibid.* **114**, 775 (2003).

[22] M. P. Brenner, D. Lohse, and T. F. Dupont, Phys. Rev. Lett. **75**, 954 (1995); D. F. Gaitan and R. G. Holt, Phys. Rev. E **59**, 5495 (1999).